Soft Matter

RSC Publishing

COMMUNICATION

View Article Online
View Journal | View Issue

Cite this: *Soft Matter*, 2013, **9**, 9755

Received 27th June 2013
Accepted 12th August 2013

DOI: 10.1039/c3sm51769a

www.rsc.org/softmatter

Effects of hydrodynamic film boundary conditions on bubble–wall impact†

Rogerio Manica,[a] Maurice H. W. Hendrix,[bc] Raghvendra Gupta,[a] Evert Klaseboer,[a] Claus-Dieter Ohl[c] and Derek Y. C. Chan*[ade]

Nanoscale interfaces among liquids, solids and gases determine the macroscopic dynamics of a bubble (*e.g.* the terminal rise velocity and bouncing behavior). Here high-speed interferograms of liquid films created from rising and bouncing bubbles are compared against mobile and immobile interface models. Quantitative agreement of the thin film dynamics with lubrication theory is obtained. Bubbles in deionized water display mobile and immobile dynamics behavior: bubble–surface interactions suggest a mobile interface but its rise velocity is reduced by the immobile bubble interface at the rear.

High speed videography has been used recently to provide detailed information about the trajectory and deformations of drop impact on a surface in air.[1–3] However, studies of collisions of bubbles rising in water with solid surfaces[4–6] focused on the bubble trajectory only. Since hydrodynamic boundary conditions at the bubble surface affect both the terminal velocity of the bubble[7] and the collision dynamics on a μm to nm scale as the bubble interacts with the surface, it is highly desirable to have accurate and consistent measurements of bubble trajectories and bubble surface interactions in the same system.

Here we present a detailed study of a rising, mm size bubble in water colliding with a glass surface after having reached terminal velocity. The bubble trajectory was tracked by high speed video. We also recorded synchronized videos of the interference fringes that form when the bubble collides with the glass surface and deforms. Quantitative information about the rate of deformation and drainage of the μm thick water film trapped between the mm sized bubble and the surface can be extracted from the interference pattern. Using measured bubble trajectory data, the evolution of the film can be modeled quantitatively with the lubrication theory to deduce the nature of hydrodynamic boundary conditions at the air–water interface.

The experimental setup[8] consists of a glass container (cross-section: 4×4 cm^2; height: 20 cm) filled with deionized Milli-Q water and covered with a glass microscope cover slip. A bubble is released from a fine needle positioned 5 mm below the glass. The bubble rises under buoyancy and reaches terminal velocity, V_T, before colliding with the glass (Fig. 1a). Its motion is recorded with a high speed video camera (SA1, Photron Inc., 54 000 fps) to furnish the bubble radius R_o and the velocity of the center of mass $V(t)$ from the side view. A second synchronized camera records the interference pattern from a laser (300 mW, Nd:YAG, $\lambda = 532$ nm) between light reflected from the glass–water and the bubble–water interfaces. Videos are available in the ESI.†

In our system, the surface tension force is dominant over the inertial force as indicated by a small Weber number, $We = 2R_oV_T^2\rho/\sigma < 1$ (see Fig. 1). Thus each bubble is, to a good approximation, a sphere with radius R_o. Here $\rho = 1000$ kg m^{-3} is the density and $\sigma = 72$ mN m^{-1} is the surface tension of the deionised Milli-Q water. The Reynolds number based on the bubble diameter and terminal velocity, Re ($= 2R_o\rho V_T/\mu$), is of the order 10^2 (see Fig. 1), where $\mu = 10^{-3}$ Pa s is the dynamic viscosity of water.

First we consider the dependence of the bubble terminal velocity, V_T, on its radius by expressing the drag force $F_{drag} = (\rho V_T^2/2)(\pi R_o^2)C_D$ in terms of the Re dependent drag coefficient, C_D. The empirical Schiller–Naumann formula, $C_D = (24/\mathrm{Re})(1 + 0.15\mathrm{Re}^{0.687})$, is accurate for $\mathrm{Re} \leq 10^3$ for a spherical bubble having a tangentially immobile boundary.[9] Thus equating the buoyancy force to the drag force, $(4\pi/3)\rho g R_o^3 = (\rho V_T^2/2)(\pi R_o^2)C_D$, gives the terminal velocity as a function of the radius. The terminal velocities for all bubbles are found to follow the Schiller–Naumann formula, inset of Fig. 1b, suggesting that the

[a]*Institute of High Performance Computing, 1 Fusionopolis Way, Singapore 138632. E-mail: D.Chan@unimelb.edu.au; Fax: +65 64630200; Tel: +65 64191111*

[b]*Physics of Fluids, University of Twente, P.O. Box 217, 7500 AE Enschede, The Netherlands*

[c]*School of Physical and Mathematical Sciences, Nanyang Technological University, Singapore 637371*

[d]*Faculty of Life and Social Science, Swinburne University of Technology, Hawthorn 3122, Australia*

[e]*Department of Mathematics and Statistics, The University of Melbourne, Parkville 3010, Australia*

† Electronic supplementary information (ESI) available: High speed videos corresponding to Fig. S1 and S2. Details of additional theoretical results and numerical calculation. See DOI: 10.1039/c3sm51769a

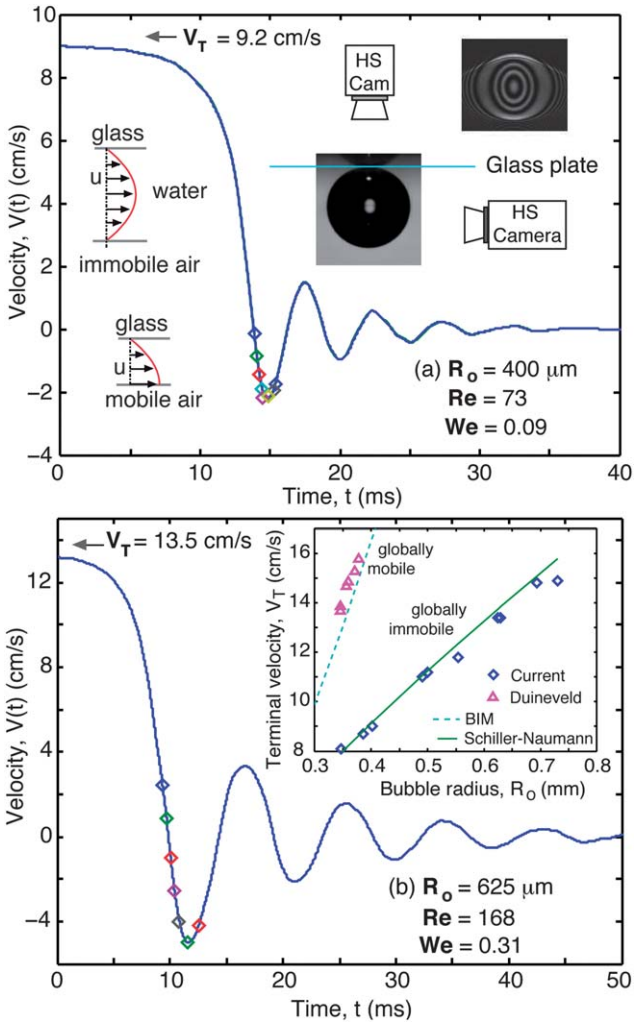

Fig. 1 (a) Measured time variation of the velocity of the center of mass of the bubble (R_o = 400 μm) approaching the glass surface. Inset: schematic of the experimental setup showing two synchronized high speed cameras recording two perspectives of the bubble–surface collision. The side view is captured with one camera while the other camera reveals the interference pattern. (b) As in (a) but for a larger bubble (R_o = 625 μm). Diamonds in the velocity curve indicate times that are plotted in the insets of Fig. 2. Inset: terminal velocity (diamonds) that obeys the Schiller–Naumann formula[9] for rigid spheres (solid line). Shown for comparison are the terminal velocities in ultra-clean water from Duineveld[7] (triangles) and numerical predictions based on the Boundary Integral Method (BIM)[10] for mobile bubbles (dashed line).

bubbles behave like rigid spheres. Bubbles of similar size rising under tangentially mobile conditions would have more than twice the speed in this size range.[7,10] The generally accepted explanation as to why bubbles exhibit a tangentially immobile boundary condition is that trace impurities are adsorbed on the bubble surface. Although we used deionized Milli-Q water, it is well known that merely trace amounts of impurities, such as those from brief exposure to the atmosphere, are sufficient to render the bubble surface immobile.[11]

Experiments using different amounts of surfactants at very low concentrations to dope ultra-clean water[5] have shown that the terminal velocity decreases with increasing surfactant dosage until it reaches that of a rigid sphere. Early work by Levich[12,13] indicates that at low surfactant concentrations, below full surface coverage, bubble motion can cause a non-uniform surface distribution of surfactants, giving rise to the Marangoni effect. The stagnant cap model[14,15] is a simple realization of this effect in which tangential hydrodynamic stress is assumed to convect the surfactants to the trailing part of the bubble surface that behaves as an immobile boundary while the leading surface is free of surfactants and is tangentially mobile with zero tangential stress. We quantify this effect in our experiments after examining results from bubble–glass collisions.

Out of over 20 bubble–glass collision experiments, we select two representative cases of bubbles with different sizes. In the main part of Fig. 1a and b, we show the velocity of the centre of mass, $V(t)$, of the two selected bubbles as a function of time as they approach the glass plate. At time $t = 0$, the bubble travels with terminal velocity V_T. In both cases, $V(t)$ decreases rapidly as the bubble approaches the glass plate. The oscillations and sign changes in the velocity are indicative of multiple bounces of the bubble at the glass plate before it comes to rest.

At around $t \sim 10$ ms, the film thickness $h \sim 10$ μm and the rate of film thinning $V_h \sim 1$ μm ms^{-1}; so we identify the film Reynolds number, $\mathrm{Re}_{film} \equiv \rho h V_h/\mu \sim 10^{-2} \ll 1$. Therefore we can use the lubrication approximation based on the Stokes–Reynolds model[16,17] in which the axisymmetric water film evolves according to $\partial_t h = 1/(3c\mu r)\partial_r(rh^3\partial_r p)$ where the constant $c = 1$ or 4 depending on whether the bubble surface is tangentially mobile or immobile. The boundary condition on the glass plate is always immobile (see the inset in Fig. 1a for a schematic velocity profile). The pressure in the film, $p(r, t)$, is determined from the Young–Laplace equation: $p + \Pi = 2\sigma/R - (\sigma/r)\partial_r(r\partial_r h)$. Here $(2\sigma/R)$ is the Laplace pressure of the bubble with $R \sim R_o$.[18] Since the disjoining pressure, $\Pi(h)$, is important only when the film has thinned down to the nm scale, it is omitted here.

To solve the coupled Stokes–Reynolds–Young–Laplace equations, knowledge of the velocity of the bubble surface outside the film is required.[18] We choose the edge of the film to be at $r_{max} = 0.7R_o$ and use the measured bubble velocity obtained from the video taken from the side at this position as input to the model. This model can then be used to predict the bubble deformation, film radius and thickness in a self-consistent manner without any fitting parameters. Numerical solutions for the tangentially mobile bubble surface boundary condition ($c = 1$) are compared with experimental data in Fig. 2a and b. Results using the tangentially immobile boundary condition ($c = 4$) differ significantly from all experimental data (see the ESI† for details).

In the main part of Fig. 2a and b, we show the evolution of the water film at the axis of symmetry: $h_o(t) \equiv h(r = 0, t)$ for the bubbles shown in Fig. 1a and b. Circles are experimental data and lines are the model predictions at the corresponding times. When the bubble approaches the glass plate from a large separation (t < 14 ms in Fig. 2a and t < 7 ms in Fig. 2b), the minimum film thickness is at $h_o(t)$. However, as the pressure in the film builds up with decreasing thickness and then exceeds the Laplace pressure of the bubble, a dimple forms. The thinnest part of the film is then at some position $r = r_m > 0$ where the

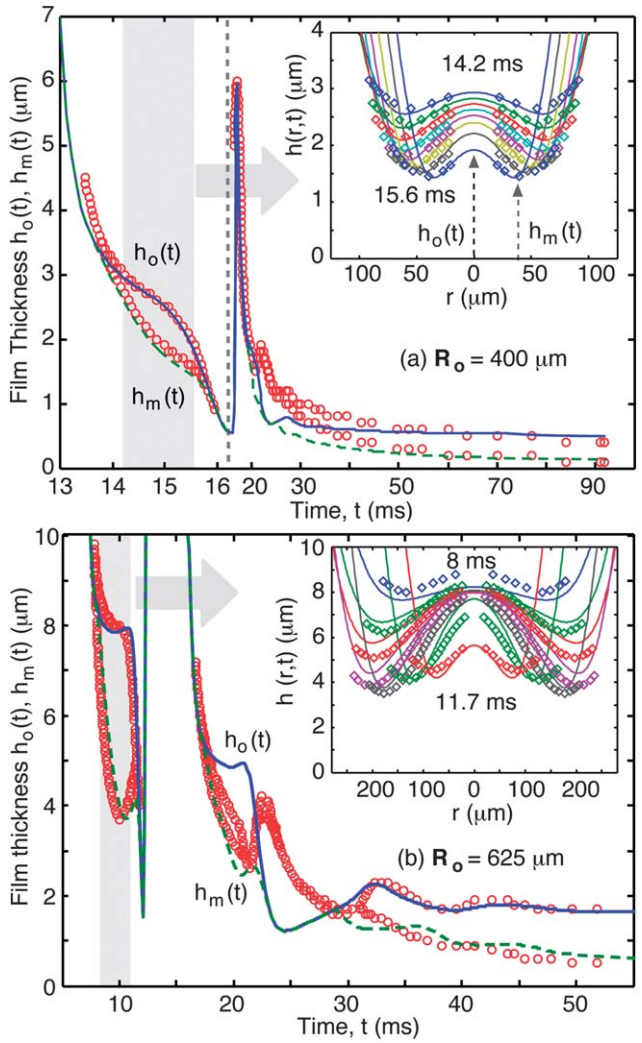

Fig. 2 Film thickness at the center, $h_o(t)$ (solid line), and at the rim, $h_m(t)$ (dashed line), for the bubbles of Fig. 1. The experimental measurements are indicated with circles. The vertical dashed line in (a) indicates a change in the horizontal time scale. The first impact occurs over a few ms while the drainage process goes on for much longer. Insets: profiles of the film thickness at selected times t_i indicated by diamonds in Fig. 1. Symbols denote experimental results and solid lines are predictions assuming a tangentially mobile bubble surface.

film thickness is $h_m(t) \equiv h(r = r_m, t)$. The dimple formation is indicated in Fig. 2a and b where the film thickness bifurcates into two branches indicated as $h_o(t)$ and $h_m(t)$ in the grey part of the time interval. The corresponding film profiles, $h(r, t)$, in this time interval are given in the insets, showing the development of the dimple in the film. The time instants corresponding to these profiles are also indicated with diamonds in the velocity–time graphs of Fig. 1a and b.

After the first collision, the bubble bounces and retreats from the glass plate and the dimple disappears, but the buoyancy force drives the bubble back towards the glass plate a second time. The film again develops a dimple as seen from the appearance of the two branches for $h_o(t)$ and $h_m(t)$ at larger times ($t \sim 20$ ms and 30 ms). Thereafter, the dimple persists as the film thins until it ruptures at $t \sim 100$ ms. The point of film rupture allows us to determine the absolute separation (see Fig. 2a and b). However, the magnitude of the first rebound is so large that fringes are not observable between the first retreat from the glass plate and the second approach. As a result, there is no experimental film thickness data available during this time interval.

Using the tangentially *mobile* bubble surface boundary condition, we are able to obtain good qualitative agreement between model and experiment for $h_o(t)$ and $h_m(t)$ as can be seen from the main plots in Fig. 2a and b. We capture dimple formation and disappearance at the first impact (in the grey part of the time interval) provided we displace all $h_o(t)$ and $h_m(t)$ values by the same constant amount to allow for the unknown displacement in the conversion from fringe order number to separation. The agreement for $h_o(t)$ and $h_m(t)$ on the second impact is not perfect, although the qualitative features are present.

The earlier observation that the terminal velocity of the bubble follows the Schiller–Naumann result (Fig. 1 inset), corresponding to a tangentially *immobile* bubble interface, can be reconciled with the fact that bubble deformation and film drainage dynamics during bubble–glass collision are consistent with a tangentially *mobile* air–water interface of the film (Fig. 2). Sadhal and Johnson[14] studied the stagnant cap model at Re = 0 and gave analytical results for the variation of the drag coefficient with the mobile cap angle, θ (Fig. 3). We have extended this result by solving numerically the steady state non-linear Navier–Stokes equation for Re = 100 for the stagnant cap model using ANSYS Fluent employing guidelines as suggested by Cuenot *et al.*[15] The variation of the drag coefficient with the mobile cap angle, θ, is shown in Fig. 3 together with the earlier results of Cuenot *et al.*[15]

We used Milli-Q de-ionized water in our experiments. However, exposure to the atmosphere is sufficient to cause trace surface active contaminants to accumulate at the bubble surface without measurable effects on the surface tension.[11] From calculations based on the stagnant cap model, a sphere with a mobile cap angle up to $\leq 60^\circ$ at the leading surface still

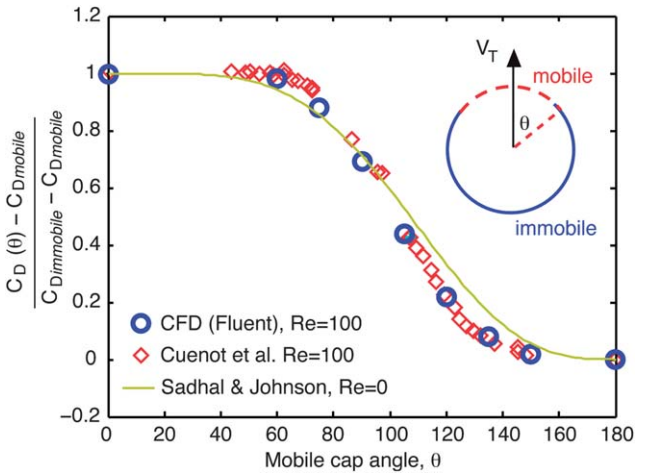

Fig. 3 Variation of the drag coefficient of a sphere with the mobile cap angle θ according to the stagnant cap model: analytical results of Sadhal–Johnson[14] at Re = 0 (line) and numerical results from the steady state non-linear Navier–Stokes equation at Re = 100 (circles).

exhibits the same terminal velocity as a completely tangentially *immobile* sphere. Such a *mobile* cap can account for the tangentially *mobile* boundary condition at the air–water interface adduced from film deformation and drainage data.

Experimental studies of the coalescence times between a rising bubble and an air–water interface found that the coalescence times depended on whether the bubble was released close or far from the interface.[19] This variation was attributed to different hydrodynamic boundary conditions caused by asymmetry of surfactant distribution due to variations in travel times and impact velocities. A quantitative comparison with this work is not possible as there was large scatter in coalescence times and the bubble dimensions and velocities were not reported.

There are a number of theoretical studies that modelled the coalescence between two colliding drops. These include, for example, effects such as internal circulation within the drops and the transport of insoluble surfactants along the drop surfaces that provided a Marangoni stress.[20–22] In our bubble–surface experiments, internal circulation effects are negligible because of the low internal viscosity of the bubble. Furthermore, within the Stokes–Reynolds model, the tangentially immobile boundary condition at the solid surface sets the upper limit of the rate of film drainage. Effects of mobile surfactants at the bubble surface only modulate the boundary condition at the bubble surface to vary between tangentially mobile and tangentially immobile, giving a maximum variation of a factor of 4 in the film drainage rate. Although surfactant transport effects cannot be excluded in modifying the second and subsequent encounters between the bubble and the glass surface, the present experimental data do not have the resolution to enable an unambiguous determination of additional model parameters such as mean surfactant concentration and surface diffusivity.

By recording simultaneously the bubble rise trajectory and the interference fringes between the glass and bubble surfaces during collision, we have accumulated data about all aspects of bubble–surface interactions. The dynamics of bubble deformation and film drainage are consistent with a tangentially *mobile* air–water interface whereas the terminal velocity of the bubble is consistent with a tangentially *immobile* surface. This dichotomy can be reconciled by the Sadhal–Johnson[14] stagnant cap model in which part of the bubble surface has been rendered tangentially *immobile* due to trace surface active contaminants arising from exposure to the atmosphere. Even though the Reynolds number Re that characterizes bubble motion is large ($\sim 10^2$), the Reynolds number that characterizes film deformation and drainage $\mathrm{Re}_{\mathrm{film}} \ll 1$, so that an axisymmetric Stokes–Reynolds–Young–Laplace model based on the lubrication theory, with input data from the bubble trajectory, can provide a quantitative account of film drainage and bubble deformation dynamics. This model contains no unknown parameters or requires further assumptions and can predict the space–time evolution of the dimensions and deformations of the μm to nm thin water film trapped between the bubble and the glass plate.

Acknowledgements

This work is supported by an Australian Research Council Discovery Project Grant. DYCC is a Visiting Scientist at IHPC. MHWH was an attachment student at NTU.

References

1 W. Bouwhuis, R. C. A. van der Veen, T. Tran, D. L. Keij, K. G. Winkels, I. R. Peters, D. van der Meer, C. Sun, J. H. Snoeijer and D. Lohse, *Phys. Rev. Lett.*, 2012, **109**, 264501.
2 J. M. Kolinski, S. M. Rubinstein, S. Mandre, M. P. Brenner, D. A. Weitz and L. Mahadevan, *Phys. Rev. Lett.*, 2012, **108**, 074503.
3 J. de Ruiter, J. M. Oh, D. van den Ende and F. Mugele, *Phys. Rev. Lett.*, 2012, **108**, 074505.
4 H.-K. Tsao and D. L. Koch, *Phys. Fluids*, 1997, **9**, 44.
5 K. Malysa, M. Krasowska and M. Krzan, *Adv. Colloid Interface Sci.*, 2005, **114–115**, 205.
6 R. Zenit and D. Legendre, *Phys. Fluids*, 2009, **21**, 083306.
7 P. C. Duineveld, *J. Fluid Mech.*, 1995, **292**, 325.
8 M. H. W. Hendrix, R. Manica, E. Klaseboer, D. Y. C. Chan and C.-D. Ohl, *Phys. Rev. Lett.*, 2012, **108**, 247803.
9 R. Clift, J. R. Grace and M. E. Weber, *Bubbles, Drops and Particles*, Academic Press, NY, 1978.
10 E. Klaseboer, R. Manica, D. Y. C. Chan and B. C. Khoo, *Eng. Anal. Bound. Elem.*, 2011, **35**, 489.
11 G. H. Kelsall, S. Tang, A. L. Smith and S. Yurdakul, *J. Chem. Soc., Faraday Trans.*, 1996, **92**, 3879.
12 A. N. Frumkin and V. G. Levich, *Zh. Fiz. Khim.*, 1947, **21**, 1183.
13 V. G. Levich, *Physicochemical Hydrodynamics*, Prentice-Hall, Englewood Cliffs, NJ, 1962.
14 S. Sadhal and R. Johnson, *J. Fluid Mech.*, 1983, **126**, 237.
15 B. Cuenot, J. Magnaudet and B. Spennato, *J. Fluid Mech.*, 1997, **339**, 25.
16 D. Y. C. Chan, E. Klaseboer and R. Manica, *Soft Matter*, 2011, **7**, 2235.
17 E. Klaseboer, J.-P. Chevaillier, A. Maté, O. Masbernat and C. Gourdon, *Phys. Fluids*, 2001, **13**, 45.
18 D. Y. C. Chan, E. Klaseboer and R. Manica, *Adv. Colloid Interface Sci.*, 2011, **165**, 70.
19 B. Jachimska, P. Warszyński and K. Malysa, *Colloids Surf., A*, 1998, **143**, 429.
20 A. K. Chesters and I. B. Bazhlekov, *J. Colloid Interface Sci.*, 2000, **230**, 229.
21 P. Santoro, Coalescence of drops with tangentially mobile interfaces: hydrodynamic effects of surfactant and ambient flow, PhD thesis, Yale University, 2007.
22 C. Vannozzi, *Phys. Fluids*, 2012, **24**, 082101.

